Fast Magnetic Fluctuations in the Solar Wind: Helios 1

F. M. NEUBAUER AND G. MUSMANN

Institut für Geophysik und Meteorologie der Technischen Universität Braunschweig, West Germany

G. DEHMEL

Institut für Nachrichtentechnik der Technischen Universität Braunschweig, West Germany

The Helios search coil experiment provides accurate low background noise measurements of interplanetary magnetic fluctuation spectra from about 4 Hz to 2.2 kHz adjacent to the frequency band from 0 to 4 Hz of the Technical University of Braunschweig flux-gate magnetometer. Apart from a slowly varying fluctuation component ranging up to 100 Hz near 1 AU and beyond 500 Hz near 0.3 AU the following superposed 'events' can be discerned in the fluctuation spectra which also have a distinct signature in the slowly varying magnetic field: (1) directional discontinuities acting as wave guide boundaries, (2) directional discontinuities producing whistler wave fields because of instability, (3) reversible magnetic field variations, mostly dips of about 1 min duration associated with whistler wave fields, (4) interplanetary shocks, where, for example, the oblique shock of January 8, 1975, has a thickness of about 1 proton gyroradius and produces an increase in whistler wave fields by more than 2 orders of magnitude in power spectral density leading to a power spectrum of 1 γ^2/Hz $f^{-3.64}$ in the wake region

INTRODUCTION

In the past decade there have been an increasing number of observational and theoretical studies on waves, discontinuities, and instabilities in the solar wind. Apart from the interest in these phenomena from the point of view of plasma physics, in which the collisionless $\beta \sim 1$ magnetoplasma of the solar wind is used as a plasma laboratory, waves and discontinuities can be used as probes of the inner regions of the interplanetary plasma down to the solar atmosphere proper. For example, Alfvén waves having periods of several hours are considered by some investigators to play an important role in the dynamics and macroscopic behavior of the solar wind by contributing wave pressure and energy transport terms. Instabilities are considered to be important for the heating and cooling and the general shaping of particle distribution functions. For a recent review, see the work by *Hollweg* [1975]. Most of these studies have been performed near 1 AU for periods well above the proton cyclotron period of 10 s for a typical magnetic field of 6 γ at 1 AU. This range of frequencies well below the appropriate ion cyclotron frequencies and of wavelengths well above the ion cyclotron radii is sometimes referred to as the magnetohydrodynamic range of wave propagation. It constitutes only a small part of the allowed range of wave propagation.

In a cold plasma with the (electron) plasma frequency f_{pe} well above the electron cyclotron frequency f_{ce}, two ranges of wave propagation exist, one extending from zero to f_{ce} and the second from about f_{pe} to infinity. No wave propagation is possible between f_{ce} and approximately f_{pe} in cold plasmas. Between the proton cyclotron frequency f_{cp} and f_{ce} the only wave mode allowed is the whistler mode with 'electronic' polarization, i.e., with a sense of polarization like gyrating electrons. The plasma of the solar wind is a hot plasma, however. Therefore it is necessary to solve the full hot plasma dispersion relations [*Montgomery and Tidman*, 1964] for the appropriate ion and electron distribution functions in order to find the propagation characteristics of plasma waves. For the solar wind case this has been done for a large number of special situations by *Fredricks and Scarf* [1965], *Barnes* [1966], *Scarf et al.* [1967], *Hamasaki* [1968], *Kennel and Scarf* [1968], *Scarf and Fredricks* [1968], *Cuperman and Landau* [1969], *Forslund* [1970], *Hollweg and Völk* [1970*a*, *b*], *Watanabe* [1970], *Pilipp and Völk* [1971], *Buti* [1973], *Baader et al.* [1973], *Rehn* [1974], *Montgomery et al.* [1975], and *Gary et al.* [1975*a*, *b*, 1976*a*, *b*]. In the solar wind case it turns out that the range from zero to the electron gyrofrequency is still the important low-frequency band of propagation for electromagnetic waves. The whistler mode or *R* mode is found to maintain its principal properties derived from cold plasma theory except for frequencies approaching f_{ce} and for large propagation angles θ between the wave vector $\mathbf{k}$ and the background magnetic field.

In the discussion of the allowed frequencies it is also important to mention the role of the Doppler effect. For a wave of frequency $f' = \omega'/2\pi$ in the plasma rest frame propagating at an angle α with respect to the solar wind velocity V_s the observed frequency is given by $f = (\omega' + kV_s \cos\alpha)/2\pi$ with the wave number k where f' and k are related to each other by the dispersion relation. If a wave number spectral density $P_k(k)$ for a magnetic field component is present in the plasma rest frame because of waves propagating at the constant angle α with respect to the solar wind speed, the power spectral density $P(f)$ observed in the spacecraft frame is given by $P(f)\,df = P_k(k)\,dk$ and

$$P(f) = 2\pi P(k)/(V_g + V_s \cos\alpha) \qquad (1)$$

where V_g is the special group velocity $(d\omega'/dk) = \mathbf{k}\cdot(\nabla_{\mathbf{k}}\omega')/k$ with the usual vectorial group velocity $\nabla_{\mathbf{k}}\omega'$.

In the plasma rest frame the power spectral density is given by $P_r(f') = 2\pi P_k(k)/V_g$ according to (1). The power spectral density at the Doppler-shifted frequency f is related to $P_r(f')$ by

$$P(f) = P_r(f')/[1 + V_s \cos\alpha/V_g(f')]$$

In comparison to $P_r(f')$ the power spectral density $P(f)$ observed by a spacecraft is reduced for $\cos\alpha > 0$. At the same

Paper number 7A0266.

time the frequency range in f is increased in comparison to f'. These effects are particularly important for waves the frequencies of which are Doppler shifted to very high frequencies above the electron gyrofrequency as f' approaches f_{ce}.

Equation (1) also shows that stationary structures in the rest frame can contribute a power spectral density $P(f) = 2\pi P(k = 2\pi f/V_s \cos\alpha)/V_s \cos\alpha$. Such structures having scale lengths less than an ion gyroradius can be realized by spatial variations in electron properties down to scale lengths of an electron gyroradius a_e in the rest frame, where $a_e = V_e/2\pi f_{ce}$ with the electron thermal speed $V_e = (2KT_e/m_e)^{1/2}$. One could then expect frequencies up to roughly

$$2\pi f_{ce} \cos\alpha \; V_s/V_e \tag{2}$$

Their structure is hinted at in the electron sheets of *Lemaire and Burlaga* [1976]. Since we cannot rule out, at least in many cases, the possible occurrence of such structures, we use the term magnetic fluctuations instead of waves in the general discussion. The observational work on fluctuations in the solar wind plasma and fields in the past has concentrated mainly on long periods above about 10 s [e.g., *Hollweg,* 1975]. Papers on observations at frequencies above the corresponding frequency 0.1 Hz up to the electron cyclotron frequency f_{ce} have been relatively infrequent in comparison.

Electric field measurements in the interplanetary plasma have been reported by *Scarf et al.* [1970*a*, 1971*a*, *b*, 1974], *Siscoe et al.* [1971], *Scarf and Siscoe* [1971], and *Scarf and Wolfe* [1974]. Magnetic observations of fluctuations in the solar wind above several hertz have been reported by *Holzer et al.* [1966] and *Scarf et al.* [1974]. The transitional range of frequencies up to 10 Hz has only recently become accessible to dc magnetometers and plasma analyzers with high sampling rates [*Fairfield,* 1974; *Unti et al.,* 1973*a*; *Neugebauer,* 1975; *Behannon,* 1975]. The fluctuation level has turned out to be so low in the range of high frequencies considered that it did not exceed the background noise levels of past wave experiments for substantial fractions of their measuring time [*Holzer et al.,* 1966; *Scarf et al.,* 1974].

In this paper we shall give an overview of some magnetic fluctuation phenomena observed by the search coil magnetometer experiment of the Institut für Geophysik und Meteorologie (IGM) of the Technical University of Braunschweig on board Helios 1. We shall concentrate here on those phenomena which also show a clear signature in the dc magnetic field which is provided by the flux-gate magnetometer experiment of the IGM. This experiment has a bandwidth of 0–4 Hz. Both experiments and almost identical ones on Helios 2 provide a unique opportunity to study electromagnetic wave phenomena in the solar wind for frequencies up to 2.2 kHz with an excellent background noise level, particularly at frequencies below 200 Hz in the radial distance range from 0.31 to 1 AU.

We shall first give a brief technical description followed by a presentation of new wave phenomena and/or correlations. More systematic studies of each of the single phenomena together with the aspect of radial variation will be presented in the future.

THE HELIOS MISSION

Helios 1 was launched on December 10, 1974, into an orbit with a period of 190 days and a perihelion of 0.31 AU. Helios 2, having almost identical instrumentation, was launched successfully on January 15, 1976, into an orbit with a perihelion of 0.29 AU.

Both spacecraft are spin stabilized with the spin axis perpendicular to the ecliptic plane and a spin period of 1 s. The data presented in this paper were obtained during the primary mission of Helios 1 from December 10, 1974, to April 24, 1975, during which the first perihelion pass took place on March 15, 1975.

INSTRUMENTATION

Detailed technical descriptions of the IGM search coil magnetometer experiment and the flux-gate experiment are already available in the works by *Dehmel et al.* [1975], *Musmann et al.* [1975], and *Gliem et al.* [1976]. We shall mention here only the most important features.

The sensor unit of the search coil magnetometer experiment consists of three orthogonally oriented search coil sensors which, together with their preamplifiers, are mounted on a boom at a distance of 4.6 m from the center of the spacecraft with the Z sensor parallel to the spin axis and the X and Y sensors in the spin plane. The wave forms from the Z sensor and one of the X and Y sensors (which one can be selected by command) are processed in an on-board spectrum analyzer. The wave form signal from each sensor first passes through eight band-pass filters which are continuous in frequency coverage and logarithmically spaced. The center frequencies f_{cn} are 6.8 Hz for channel 1 and 14.7, 31.6, 68, 147, 316, 681, and 1468 Hz for the following channels. A novel feature of the instrument is that the filter outputs are not processed by some analog device but by a digital mean value computer.

After fast A/D conversion using two ranges for every frequency channel the mean square M_n is digitally computed for adjacent time intervals, the lengths of which depend on the bit rate. In addition to the mean square of the filter output M_n for a given averaging interval τ_{ave} the peak value is obtained to be transmitted to the ground. The averaging time τ_{ave} can vary between 1.125 s and roughly 20 min for total data transmission rates from 4096 bps (bits per second) down to 8 bps. Real-time transmission is possible in four different formats. For most of the primary mission of Helios 1 a data rate of 2048 bps was available for the total payload with $\tau_{ave} = 1.125$ s.

The mean value computer guarantees the accurate determination of average spectral densities in each filter channel. This was not always guaranteed for the analog devices used in the past. If $T_n(f)$ is the complex transfer function of channel n with $T_n(f_{cn}) = 1$ at the center frequency f_{cn}, the mean square value M_n computed in the spectral analyzer is related to the power spectral density $P(f)$ of the magnetic field by

$$M_n = \int_0^\infty f^2 P(f) |T_n(f)|^2 \, df \tag{3}$$

In (3) the search coil output is proportional to the time derivative of the magnetic field at least well below the resonance frequency, which in our case is at 3 kHz. The frequency response of filter n expressed by $T_n(f)$ is flat around the center frequency f_{cn}. The lower and upper frequency limits of a band filter, f_{ln} and f_{un}, respectively, are characterized by $|T_n(f_{ln})| = |T_n(f_{un})| = 1/(2)^{1/2}$. The upper frequency limit f_{un} of filter n is equal to the lower frequency limit f_{ln+1} of filter $n + 1$. These frequencies are 4.7 Hz, 10 Hz, 22 Hz, 47 Hz, 100 Hz, 220 Hz, 470 Hz, 1 kHz, and 2.2 kHz. In addition, the filters have been designed such that

$$\int_0^\infty |T_n(f)|^2 \, df \approx f_{un} - f_{ln}$$

with high accuracy for all filters $n = 1, 2, \cdots, 8$.

A weighted average of the power spectral density $\langle P_n \rangle$ over the frequency band of filter n or the spectral density $\langle P_n \rangle^{1/2}$ can then be computed according to

$$M_n = (f_{un} - f_{ln}) f_{cn}^2 \langle P_n \rangle \quad (4)$$

By using (3) and (4) and the above-mentioned filter characteristics the following important property can be deduced: the error due to the weighting by $|T_n|^2 f^2$ essentially disappears for a power spectrum with an f^{-2} dependence if we assign the value $\langle P_n \rangle$ to the center frequency f_{cn}. Even for very steep spectra the errors due to $|T_n|^2 f^2$ are very small in comparison with the dynamic range of about four decades in spectral density given in $\gamma/(\text{Hz})^{1/2}$. The dynamic range can be extended by a commandable gain change amplifier. The numerical peak values are given such that for a monochromatic signal the ratio of peak value divided by mean value is $(2)^{1/2}$.

In addition to the spectral analyzer data it is also possible to transmit three-component wave form data at sampling rates of 28.5 and 57 samples per second in real time and 75, 150, and 300 samples per second in a memory mode. Since these data are not used in this paper, we shall not discuss the wave form channel further.

An important point is the question of the background noise levels. On January 18, 1975, there was a rare opportunity to study the steady experiment background noise levels when the measured fluctuation levels decreased to stay at constant levels for several hours. Figure 1 shows the 40-s-average noise spectrum representative for several hours of data for the components Y and Z used exclusively during the primary mission. For the channels 1Y and 1Z the equivalent number of degrees of freedom is 424. Here we have defined the equivalent number of degrees of freedom by $2 \cdot (f_{un} - f_{ln}) \cdot \tau_{\text{ave}}$, where $\tau_{\text{ave}} = 40$ s. It turns out that the fluctuation levels of the Y component essentially agree with the preflight measurements of the sensor-preamplifier system. We conclude that for the Y component the background noise levels contain no contribution from the spacecraft. This is somewhat different for the Z component where a small hump is seen for channels 2Z and 3Z. These noise densities above the sensor noise levels are probably due to magnetic stray fields from the solar array at the frequency 16 Hz as well as the first and possibly the second harmonic at 32 and 48 Hz. The frequency of 16 Hz is due to the 16 solar panel segments around the spacecraft. The very low stray field levels from the solar array demonstrate the careful wiring of the solar panels (see, for example, *Scarf et al.* [1974]). For comparison, Figure 1 also shows the noise levels for the Imp 6 single-loop magnetic wave experiment, the Hawkeye 1 search coil experiment (D. Gurnett, personal communication, 1976), and the Ogo 5 search coil experiment [*Frandsen et al.*, 1969]. Below about 200 Hz the noise levels for the Helios search coil experiment are lower than the Imp 6 and Hawkeye 1 experiment noise levels, and above 200 Hz they are greater. The Ogo 5 noise values are a little above the Helios 1 Y curve up to several hundred hertz where they start to bend strongly upward because of the lower resonance frequency. Note that in designing a magnetic wave experiment there is a trade-off between bandwidth and noise quality in addition to other trade-offs. Also shown are the background noise levels reported by *Scarf et al.* [1974] for Imp 7. They have been attributed to solar panel stray currents by these authors, although electromagnetic interference seems to be another possibility. Since on almost every day of the Helios 1 mission the interplanetary

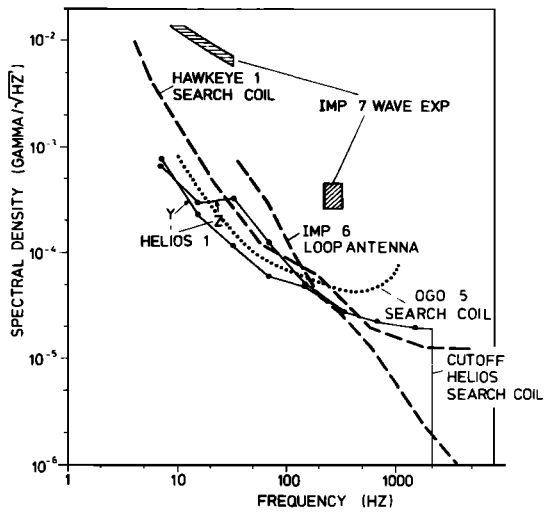

Fig. 1. Background noise levels of various magnetic wave experiments in comparison with the values for the Y and Z components of the Helios 1 search coil experiment determined in flight.

fluctuation level decreased to values below the background noise levels shown in Figure 1, at least for a few minutes, it has been verified that apart from minor changes, Figure 1 is representative for the complete primary mission. A further search for spacecraft noise of short duration has led to only one nominal spacecraft operation resulting in a short spike ascribed to spacecraft stray fields. We note finally that the strong signals associated with the spin of 1 Hz in a constant ambient field are well below the spectrum analyzer noise levels because of the strong removal of low frequencies by appropriate filtering.

The flux-gate experiment also used for this investigation consists of a triaxial orthogonal sensor system of the Förster type mounted on the same boom as the search coil at a distance of 2.8 m from the center of the spacecraft. In its sensitive range of ± 102.4 γ for each component it has a digitization uncertainty of ± 0.2 γ. Since the maximum sampling rate is 8/s, it includes an aliasing filter having a corner frequency of 4 Hz. During most of the primary mission it provided four vectors per second. The data are corrected for possible misalignments, zero offsets in the spin plane, etc. Only the very slowly varying zero offset for the Z component has not been corrected yet; thus there is an uncertainty of at most ± 2 γ at the present time.

General Results

The magnetic fluctuation fields observed by this search coil experiment generally consist of a slowly varying broadband background with superposed 'events' of various kinds. The slowly varying component can be defined as having a time scale of roughly 10 min or longer. Figure 2 shows a typical example for the appearance of the slowly varying interplanetary background near 1 AU. One hour of data is shown for the Y component and an averaging time of 8 s. Spectral density values are presented together with peak values as the lower and upper end, respectively, of a vertical bar at each time on a logarithmic scale. In addition, the distance from the sun is shown. Even near 1 AU where the wave fields have their lowest intensity the spectral densities are generally well above the background noise levels for the four lowest channels extending up to 100 Hz. On a typical 1-hour plot the slowly

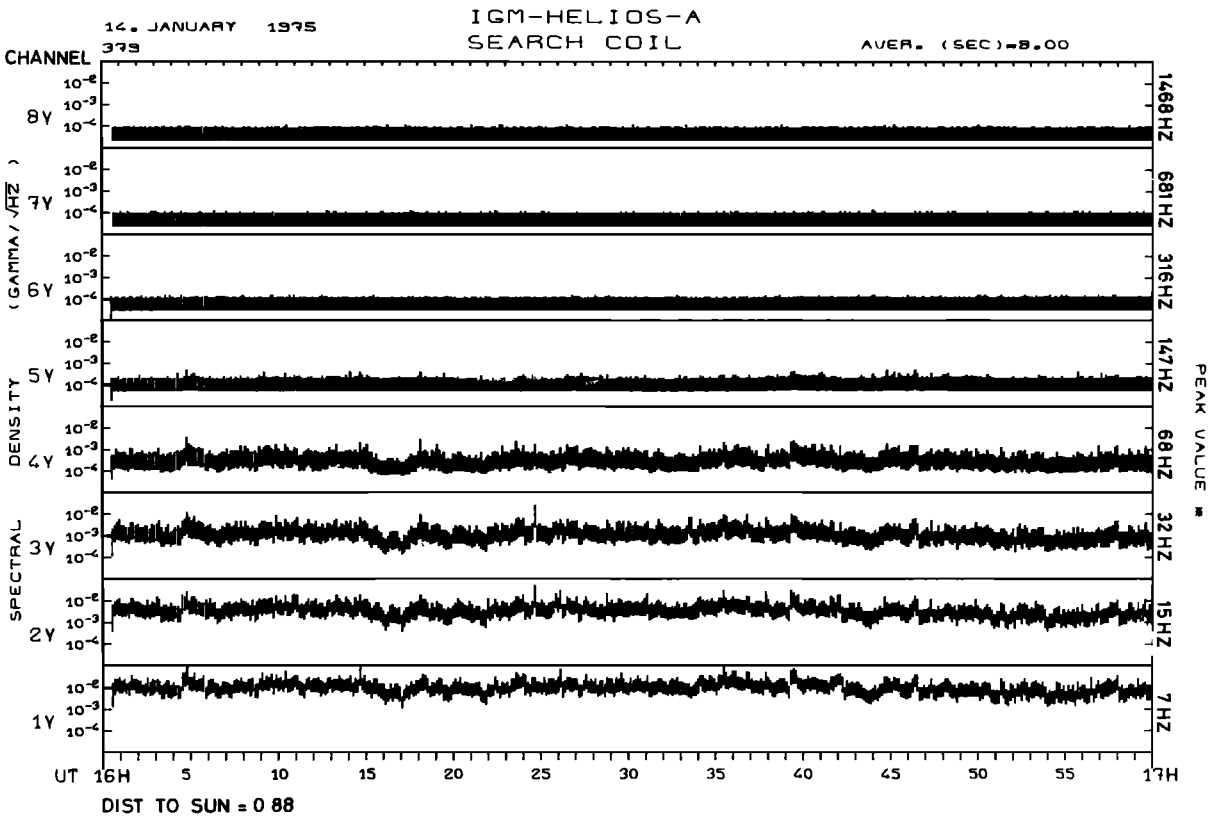

Fig. 2. A typical 1-hour interval of magnetic fluctuation spectra on January 14, 1975, at 0.88 AU from the sun. For further explanation see text.

varying component together with the superposed events leads to variations of 1–2 orders of magnitude in spectral density.

We will mention a few important properties of the slowly varying background magnetic fluctuation fields [*Neubauer et al.*, 1977; *Beinroth and Neubauer*, 1976; *Beinroth et al.*, 1976] before entering the analysis of typical events. Near 1 AU, typical spectral densities of 10^{-3}–$10^{-2}\gamma/(\mathrm{Hz})^{1/2}$ at 7 Hz and 10^{-4} $\gamma/(\mathrm{Hz})^{1/2}$ around 70 Hz are typical. During one solar rotation, variations in spectral density of the slowly varying component by 1–2 orders of magnitude are observed. As the sun is approached, the spectral density levels shift upward by more than 1 order of magnitude. We shall now present various types of events superposed on the slowly varying background.

Directional Discontinuities

Directional discontinuities [*Burlaga*, 1968], or 'current sheets' [*Siscoe et al.*, 1968], have been investigated in a number of papers during the past 9 years. They are characterized in the magnetic field by a discontinuous change in the magnetic vector direction generally associated with only a minor change in magnitude. By discontinuity is meant a sharp transition which passes by the spacecraft in a time of the order of a few seconds (30 s in the work by *Burlaga* [1968]).

Discontinuities having the above characteristics have been identified as tangential discontinuities and rotational discontinuities [e.g., *Burlaga*, 1971; *Burlaga et al.*, 1976; *Smith*, 1973; *Solodyna et al.*, 1977]. A general tangential discontinuity must conserve total pressure and must have a vanishing normal component of the magnetic field. It does not propagate with respect to the plasma. Apart from these conditions the jumps are arbitrary. Most observed tangential discontinuities are characterized by changes in magnetic field direction only. In contrast, a rotational discontinuity propagates. It has a nonzero normal component of the magnetic field, and a well-defined relationship exists between the change in magnetic field and velocity vectors across the discontinuity.

The structure of the transition layer between both sides of a discontinuity can only be described by kinetic theory. For tangential discontinuities this has been done by *Lemaire and Burlaga* [1976]. With respect to the wave fields in the solar wind we can immediately predict two possible roles for these structures. First, the refractive index surface at each frequency will undergo appreciable changes through the discontinuity. Hence, as is the case for whistler duct boundaries in the terrestrial magnetosphere [*Helliwell*, 1965], waves may be reflected or transmitted through discontinuity structures depending on their initial conditions. From this ducting alone we would expect abrupt changes in wave activity at a discontinuity.

Note that under solar wind conditions the transmission properties of tangential discontinuities for whistler waves depend on the details of the transition layers which are sometimes very complex. This can easily be seen by observing that the wavelength $\lambda = c/(nf)$ of whistler waves is much less than the thickness of tangential discontinuities, which has been observed generally to exceed 1 proton Larmor radius [*Burlaga et al.*, 1976] in the solar wind.

The discontinuity may play a second role as an unstable structure. An interesting candidate for destabilization may be the currents flowing in a discontinuity to produce the observed change in magnetic field vectors. For purely directional tangential discontinuities the current would be strictly field

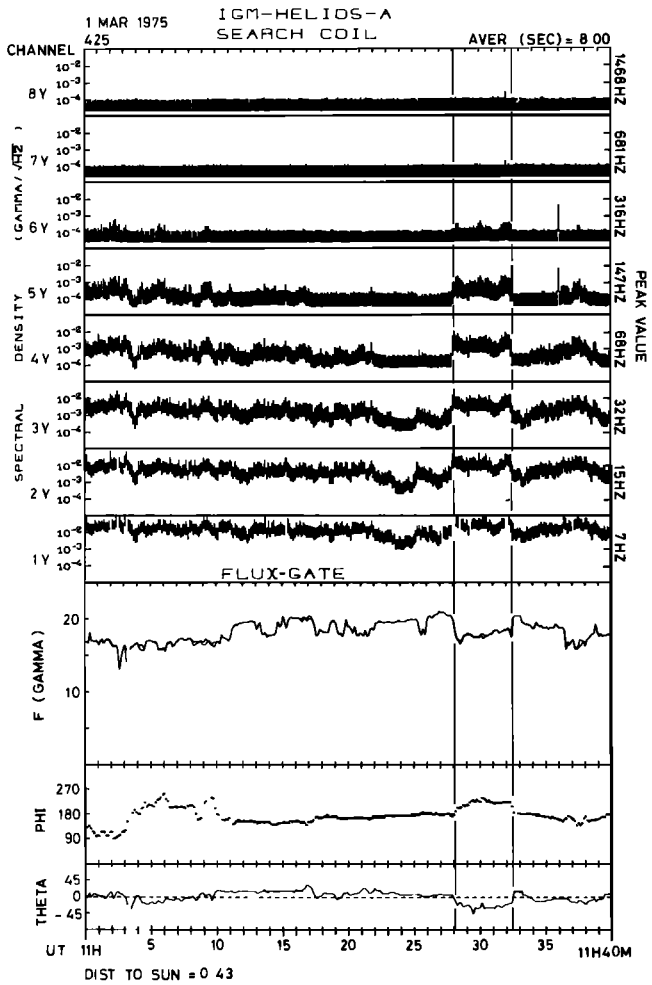

Fig. 3. Example of two interplanetary discontinuities (vertical lines) acting as a wave guide. For further explanation and discussion see text.

aligned. If such a current instability occurs, the waves produced may behave very differently depending on the geometry of the discontinuity and the propagation characteristics outside the source region, i.e., the discontinuity. In most cases we shall expect a maximum in the wave fields observed in the source region.

Both types of behavior have been observed in connection with directional discontinuities in the solar wind. Figure 3 shows ducting in a wave guide produced by a pair of discontinuities in magnetic field direction at 1128 and 1133 UT. The lower panels of the figure show the magnetic field vectors averaged over 8 s represented by the magnitude and the usual solar ecliptic angles. For the magnitude F two different averages are drawn, the magnitude resulting from the averaged individual components and the average of the individual magnitudes. The spectral data for 8-s averaging intervals are shown in the upper panels in the same format as in Figure 2. The discontinuities are identified as tangential ones, since the magnetic field magnitude changes appreciably across each of them. Note that in channels 2–4, increases in wave intensity by an order of magnitude in spectral density occur which are very accurately limited by the vertical bars denoting the discontinuities. The increase extends at least to channel 6, i.e., to the range 220–470 Hz. The electron cyclotron frequency is about 500 Hz between the discontinuities. If we assume that the waves propagate roughly parallel to the magnetic field, there will be only a small Doppler shift at $f_{ce}/2$ because of the maximum in phase velocity. Hence the wave spectrum extends at least to $f_{ce}/2$ with a spectral index $\gamma = 1.2$ in $[P(f)]^{1/2} \sim f^{-\gamma}$. Note also that outside the wave guide above channel 3 the background noise is measured. The ducting property of directional discontinuities is not a rare phenomenon but occurs for a large fraction of directional discontinuities. The only way to avoid the interpretation in terms of ducting is to assume an extremely narrow cone of propagation wave vectors around the magnetic field vectors such that no spreading of the wave field across the boundaries of the discontinuities occurs. The wave fields must have their source between the discontinuities in such a case.

A directional discontinuity is also observed very often as a source of waves. An example is shown in Figure 4. The fluxgate vector data for the directional discontinuity are presented in a coordinate system spanned by the eigenvectors from a variance matrix analysis of the *Sonnerup* [1971] type applied to the transition layer from 0719:51 to 0720:01 indicated by the two vertical lines. The normal direction is given by $\mathbf{n} = (-0.232, 0.807, 0.543)$ in solar ecliptic coordinates.

$B(3)$ is the component in the normal direction. The figure shows the magnetic field components as a function of time with four vectors per second. Figure 5 shows the hodograph in the discontinuity plane. During the transition the magnetic field decreases from 4.8 to 3.9 γ. The small component $B(3)$ together with the relatively large decrease in magnitude suggests that the directional discontinuity is a tangential one.

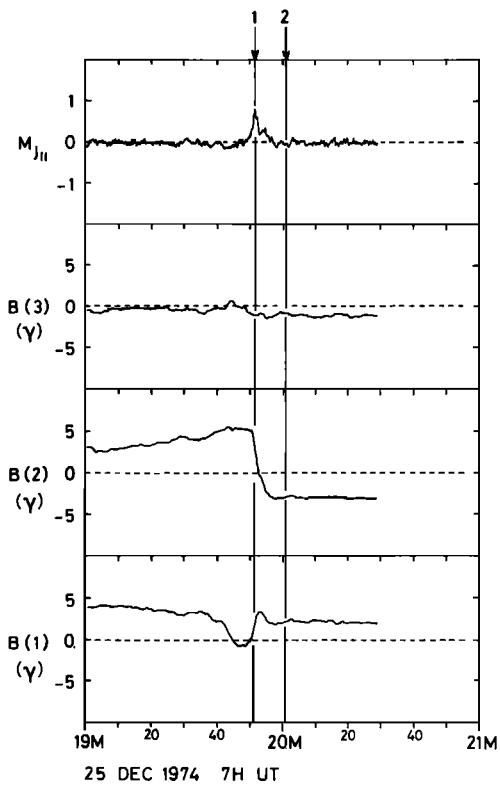

Fig. 4. Interplanetary tangential discontinuity in a coordinate system of minimum variance eigenvectors. $B(3)$ is the component in the direction of minimum variance. The variance analysis interval is shown by vertical lines. $M_{J_{II}}$ is the Alfvén Mach number of the relative speed between electrons and protons, i.e., relative speed divided by Alfvén speed computed according to (5).

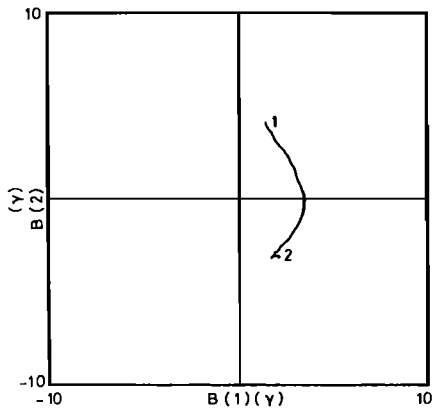

Fig. 5. Hodograph of discontinuity magnetic fields in a plane perpendicular to the minimum variance eigenvector. The discontinuity is the same as in Figure 4.

Note also that the structure preceding the analysis interval agrees with the picture of a tangential structure.

The associated wave fields are presented for channels 1Y–5Y and an averaging time of 1.125 s in Figure 6. There is a strong peak in wave activity by a factor of about 20 in channel 2Y from 10 to 22 Hz and by at least a factor of 10 from 22 to 47 Hz. Channels 5Y–8Y show background noise only. The average magnetic field of approximately 4.5 γ corresponds to an electron cyclotron frequency of 126 Hz. The slowly varying background also increases slightly during the event. There is a broad peak by a factor of about 5 in the lowest channel, 1Y. Before the time of the peaks, only background noise is observed above 10 Hz. Altogether the spectrum is flat until it starts to decline between 15 and 32 Hz.

By using the magnetic field structure as resolved by a fast sampling magnetometer and plasma analyzer the current density could be computed. Also for the stability analysis the relative speed of ions and electrons in relation to the critical drift speeds of various instabilities is of interest. If the solar wind speed is $\mathbf{V}_s$, the spatial derivative in the direction of the normal $\mathbf{n}$ of a tangential discontinuity is

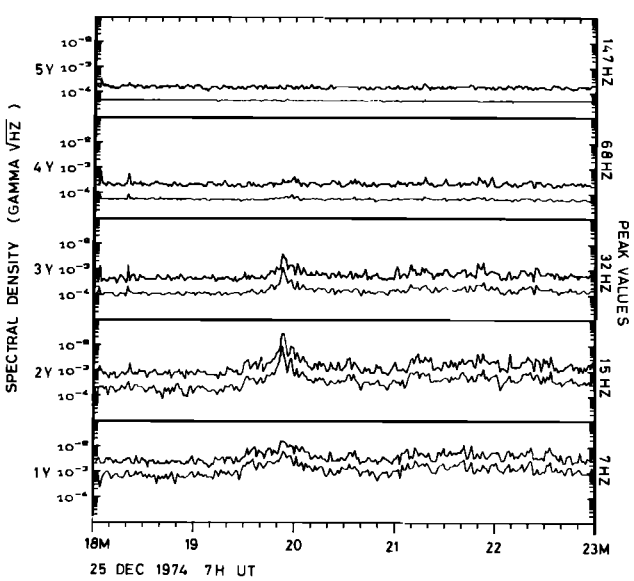

Fig. 6. Magnetic fluctuation spectra for the tangential discontinuity of Figures 4 and 5.

$$(d/dn) = -(\mathbf{V}_s \cdot \mathbf{n})^{-1}(d/dt)$$

The curl of the magnetic field is given by

$$\text{curl } \mathbf{B} = -(1/\mathbf{V}_s \cdot \mathbf{n})\mathbf{n} \times \dot{\mathbf{B}}$$

The field-aligned relative velocity between protons and electrons, α particles being neglected, in relation to the Alfvén speed b is then given by the relation

$$M_{J\parallel} = \frac{V_{\parallel,p} - V_{\parallel,e}}{b} = \frac{1}{M_A} \frac{\mathbf{n} \cdot (\mathbf{B} \times \dot{\mathbf{B}})}{\omega_{ci} B^2} \frac{1}{\cos \alpha} \tag{5}$$

where α is the angle between the solar wind direction and the normal $\mathbf{n}$ and M_A is the Alfvén Mach number of the solar wind speed $|\mathbf{V}_s|$. The solar wind plasma properties enter only via the Alfvén Mach number $M_A = V_s/b$ and $\cos \alpha$. Note also that the product $M_A \cdot \omega_{ci}$ does not depend on the magnetic field. If the current is mostly field aligned, the electron average speed is given by

$$\mathbf{V}_e \approx \mathbf{V}_s - M_{J\parallel} \cdot b \cdot \mathbf{B}/B \tag{6}$$

For our special case, $M_{J\parallel}$ is shown in the upper part of Figure 4. $M_{J\parallel}$ has a maximum which coincides with the wave maxima in Figure 6 at 2052. The plasma parameters have been provided by the Helios plasma experiment [*Schwenn et al.*, 1975; H. Rosenbauer, personal communication, 1976]. Since one proton-electron spectrum is obtained every 40.5 s, the fine structure of the discontinuity cannot be resolved, although the flux values contributing significantly to the calculation of the plasma bulk properties are collected within a much shorter interval. At the maximum we have $M_{J\parallel} = +0.8$, i.e., the relative bulk speed of protons and electrons is 0.8 times the Alfvén speed. Although a detailed analysis of the stability properties of the plasma in the transition layer would require additional information on the exact shape of the particle distribution functions as a function of location, the following physical picture seems to be plausible: the tangential discontinuity has reached a state where the waves excited by the current instability have stabilized the plasma to such an extent that the gain in wave energy by the instability compensates for the energy losses due to absorption and/or propagation. The thickness of the structure analyzed is about 1250 km. With a measured proton temperature of $T_i = 176.000$ K we obtain a thermal proton gyroradius of $(2KT_i/m_i)^{1/2}/\omega_{ci} \approx 125$ km leading to a thickness of about 10 thermal proton gyroradii, which is much thicker than the most probable value according to a scan of discontinuities in Helios data as well as earlier results [*Burlaga et al.*, 1976]. We note also that in the example discussed here a small perpendicular current component must be present because of the variation in magnetic field magnitude.

Although we cannot rule out the possibility of convected electron structures, we interpret the search coil observations in terms of whistler waves driven unstable inside the discontinuity. First, we take the case of the protons $\beta_i = 8\pi NKT_i/B^2 \approx 1.5$, $T_i \approx T_e$, and the Alfvén speed $b \approx 43$ km/s. Near the maximum of $M_{J\parallel}$ we have the magnetic field in solar ecliptic components (2.9, 0.9, 2.0) γ. We note that the maximum current is flowing parallel to $\mathbf{B}$, i.e., toward the sun.

After having collected these numerical values we discuss the whistler mode instability. In a recent theoretical paper, *Gary et al.* [1976*b*] discuss instabilities due to field-aligned currents in a $\beta_i \approx 1$ plasma characteristic of the solar wind. They show that the whistler mode is driven unstable by resonant protons which have to move somewhat faster than the wave to see the correct sense of polarization. The unstable wave has to propa-

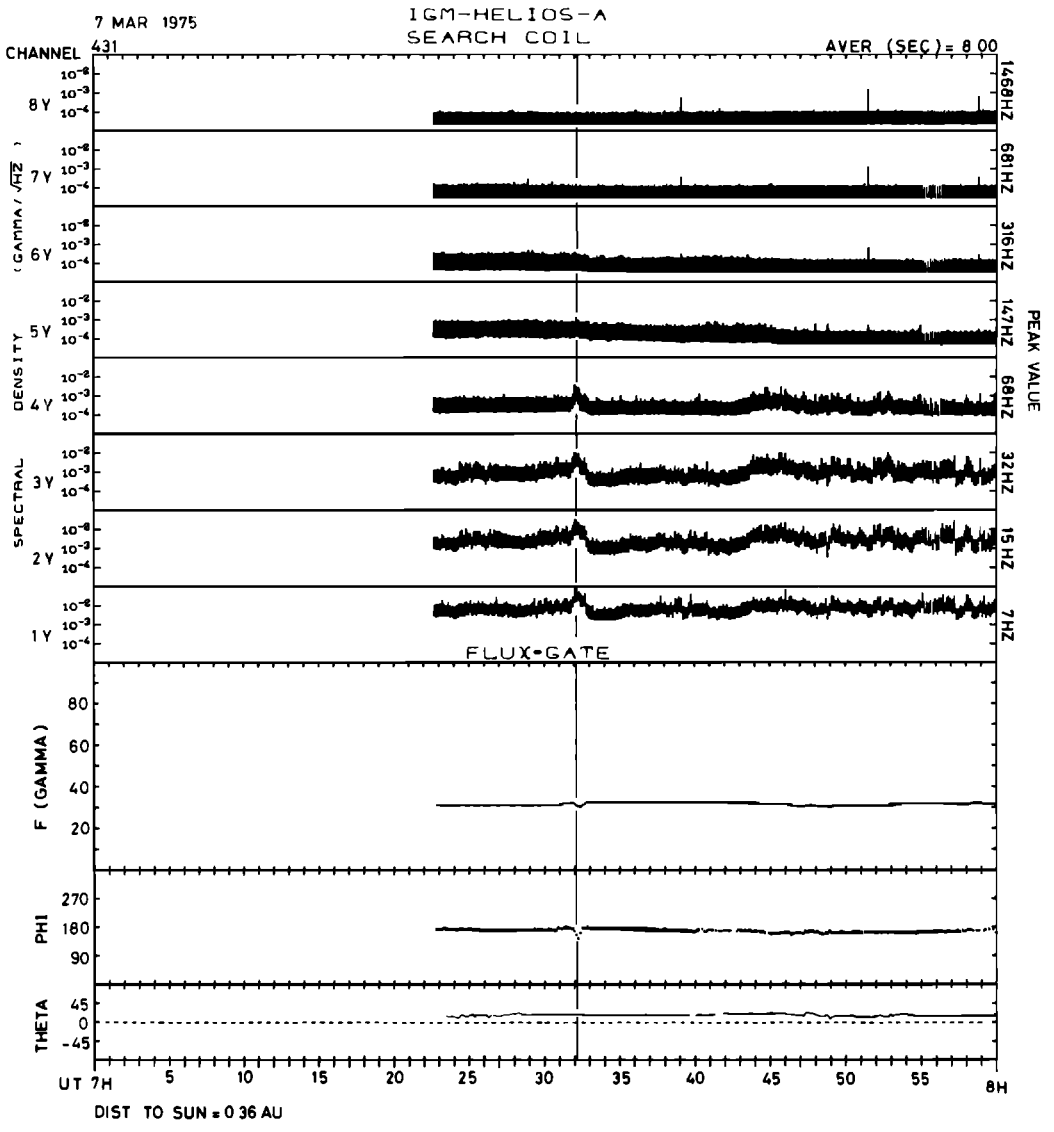

Fig. 7. Example of a reversible magnetic field structure with a peak in the fluctuation spectra up to at least channel 4Y (47–100 Hz).

gate in the current direction. They also show that the instability is strongest for propagation parallel or antiparallel to the magnetic field. The real part of the frequency is given by the cold plasma dispersion relation in the electron frame of reference. In our case this is the frame moving with $\mathbf{V}_e$, and the waves must propagate in the **B** direction. Because of the relatively low Alfvén speed, Doppler shifts play an important role. Nevertheless the observations show that in our case the waves extend to much higher frequencies than the unstable waves of *Gary et al.* [1976*b*]. If the interpretation in terms of unstable whistler waves is accepted, this leads to the conclusion that the electron and ion distribution functions cannot be shifted isotropic Maxwellians as was assumed by *Gary et al.* [1976*b*] but must deviate appreciably from such idealized situations. Although no observations are available concerning this point, it does not seem unreasonable to assume that apart from the current the particle distribution functions deviate from isotropic Maxwellians at least as much as the usual distribution functions in the less disturbed solar wind between the discontinuities. Finally, we mention the possible role of wave-wave coupling near the spectral density peak to account for the extension of the spectrum to higher frequencies than were predicted by *Gary et al.* [1976*b*]. Further discussion and analysis of these aspects will be presented in the future.

Short Reversible Variations in the Magnetic Field

Here we discuss a structure which generally has a duration of about 1 min and which occurs several times per day. It is characterized by a fast variation of the magnetic field vector with a subsequent return to the initial magnetic field configuration. During the variation an extremum of the magnetic field magnitude, usually a minimum, is reached. A particularly clean example is shown in Figure 7. The event is embedded in a very quiet magnetic field. It is connected with a broadband maximum in whistler mode activity by more than 1 order of magnitude above the surrounding 'continuum.' The increased wave activity extends beyond the boundaries of the event. Figure 8 shows the vector magnetic field variations for maximum time resolution, i.e., four samples per second. We have used the representation in solar ecliptic components. Considering the hodograph of this structure, one finds that the tip of the magnetic field vector moves back and forth along a straight

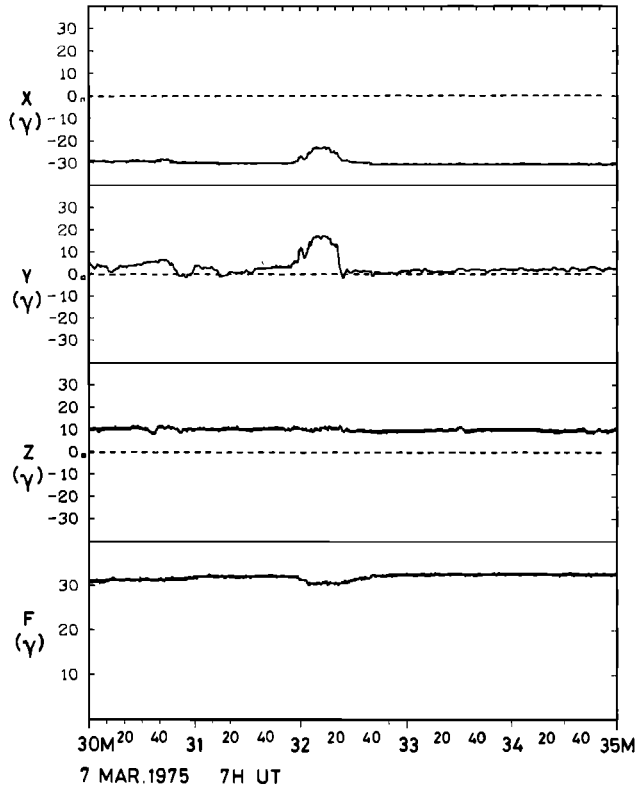

Fig. 8 Reversible structure of Figure 7 shown with a resolution of four vectors per second. Note the steep gradients in the magnetic field components.

line. In a magnetohydrodynamic framework the structure could be a convected region of excess plasma pressure with an essentially constant profile or a propagating structure with a nonstationary profile.

The structure just described is probably a weak example of a type of 'magnetic hole' reported from dc magnetometer observations alone by *Turner et al.* [1976]. We note that the structure is much more dramatic in the high-time-resolution observations than in the low-time-resolution data. Apart from a change in the continuum level for frequencies up to at least 220 Hz we see peaks in wave activity for frequencies extending beyond 47 Hz. Closer inspection reveals a small but clear increase at 0724 in the lowest three channels which also extends into the frequency range covered by the flux gate, i.e., below 4 Hz. The high-time-resolution vector data in Figure 8 show fairly strong gradients. Finally, we note fluctuation fields in the flux-gate data from 0740 to 0742 and from 0746 to 0800. Their amplitudes are a few gammas. In the search coil data wave activity extending up to channel 4Y starts at about 0744.

SHOCK OF JANUARY 8, 1975, AT 0022:09 UT

Shocks are among the most dramatic events in the fluctuation spectra. In the past, interplanetary shocks have been investigated almost solely from the macroscopic point of view as major interplanetary disturbances. High-time-resolution observations of shock wave fields can yield important information on the plasma physics of these structures. So far, it has been almost exclusively the earth's bow shock which has been investigated from this point of view [*Fredricks et al.*, 1968, 1970*a*, *b*, 1971, 1972; *Olson et al.*, 1969; *Scarf et al.*, 1970*b*, 1971*b*; *Holzer et al.*, 1972; *Formisano and Hedgecock*, 1973*a*, *b*; *Formisano*, 1974; *Fairfield*, 1974; *Fairfield and Feldman*, 1975; *Rodriguez and Gurnett*, 1975; *Formisano et al.*, 1975; *Greenstadt et al.*, 1975]. One study of high-frequency magnetic fluctuations in the vicinity of an interplanetary shock has been published by *Unti et al.* [1973*b*]. An advantage of using interplanetary shocks for such studies is the relative ease with which the measured temporal variations can be converted into spatial variations, an omnipresent problem in bow shock studies.

The relatively rare occurrence of interplanetary shocks compared with the number of bow shock crossings is a disadvantage. Another disadvantage is the high wave form sampling rate required for resolving these structures. We mention in this respect that for extended time periods during the Helios mission, real-time vector wave form data are available at sampling rates of up to 57 Hz corresponding to a Nyqvist frequency of 28.5 Hz. In addition, in a memory mode, wave form data at sampling rates of 75, 150, and 300 Hz for time intervals selected by an on-board event detector can be obtained. However, such data were not available for this study.

From the shocks observed during the primary mission of Helios 1 we shall present here the magnetic field data for the shock of January 8, 1975, at 0022:09 UT. In this paper we treat the microscopic aspects only. Figure 9 shows the combined flux-gate magnetic field data and search coil spectral data for the 1-hour interval around the shock. The jump in magnitude from 8 to 14 γ is associated with increases in spectral density by more than 1 order of magnitude in channels 1Y–4Y and by at least a factor of 2 in channel 5Y extending from 100 to 220 Hz. The magnetic field in front of the shock is very quiet both in the flux-gate data and in the spectral data which show the background noise apart from the directional discontinuity near 0015. In the lower channels 1Y and 2Y the shock is preceded by wave fields for at least 100 s in channel 1Y and at least 30 s in channel 2Y. These precursors are absent or below the experiment noise level in the channels above 2Y.

We shall now compute the macroscopic properties of the shock required for the kinetic analysis. Since a discontinuity occurs at 0015, we use the time interval 0015:00–0021:40 to compute the average magnetic field vector $\mathbf{B}_1$ in front of the shocks and obtain $\mathbf{B}_1 = (-6.26, -0.94, 4.93)\ \gamma$. The time interval 0022:20–0029:00 yields $\mathbf{B}_2 = (-6.24, +4.55, 11.6)\ \gamma$ and $\Delta\mathbf{B} = \mathbf{B}_2 - \mathbf{B}_1 = (0.02, 5.49, 6.67)\ \gamma$.

In order to determine the shock normal we use the coplanarity theorem, which is known to be of limited accuracy in the general case. In our example its use seems to be rather promising, since there are only small magnetic field gradients during the averaging times on both sides of the shock. An error source which we have to consider is the as yet unknown zero offset in the Z component of maximum $\pm 2\ \gamma$. It turns out not to be serious, however. Applying the coplanarity theorem to $\mathbf{B}_1$ and $\mathbf{B}_2$, we obtain $\mathbf{n} = (-0.852, -0.404, +0.335)$ or, expressed in angles, $\phi_n = 205 \pm 8°$ and $\theta_n = 19 \pm 5°$, where the errors given are due to the unknown offset (spacecraft field plus sensor offset) in the Z direction.

To convert the shock time scale into a distance scale, it is necessary to determine the shock speed in the direction of $\mathbf{n}$. Averaging over 10 plasma spectra each from 0015:13 to 0021:58 and from 0022:38 to 0029:23, we obtain $N_1 = 4.04$ cm^{-3} and $N_2 = 7.16$ cm^{-3} for the proton concentrations ahead of and behind the shock, respectively. Taking into account the α particle contribution, we obtain $b_{n,1} = 73$ km/s for the Alfvén speed based on the normal magnetic field. The shock jump relations then yield the propagation speed in the rest

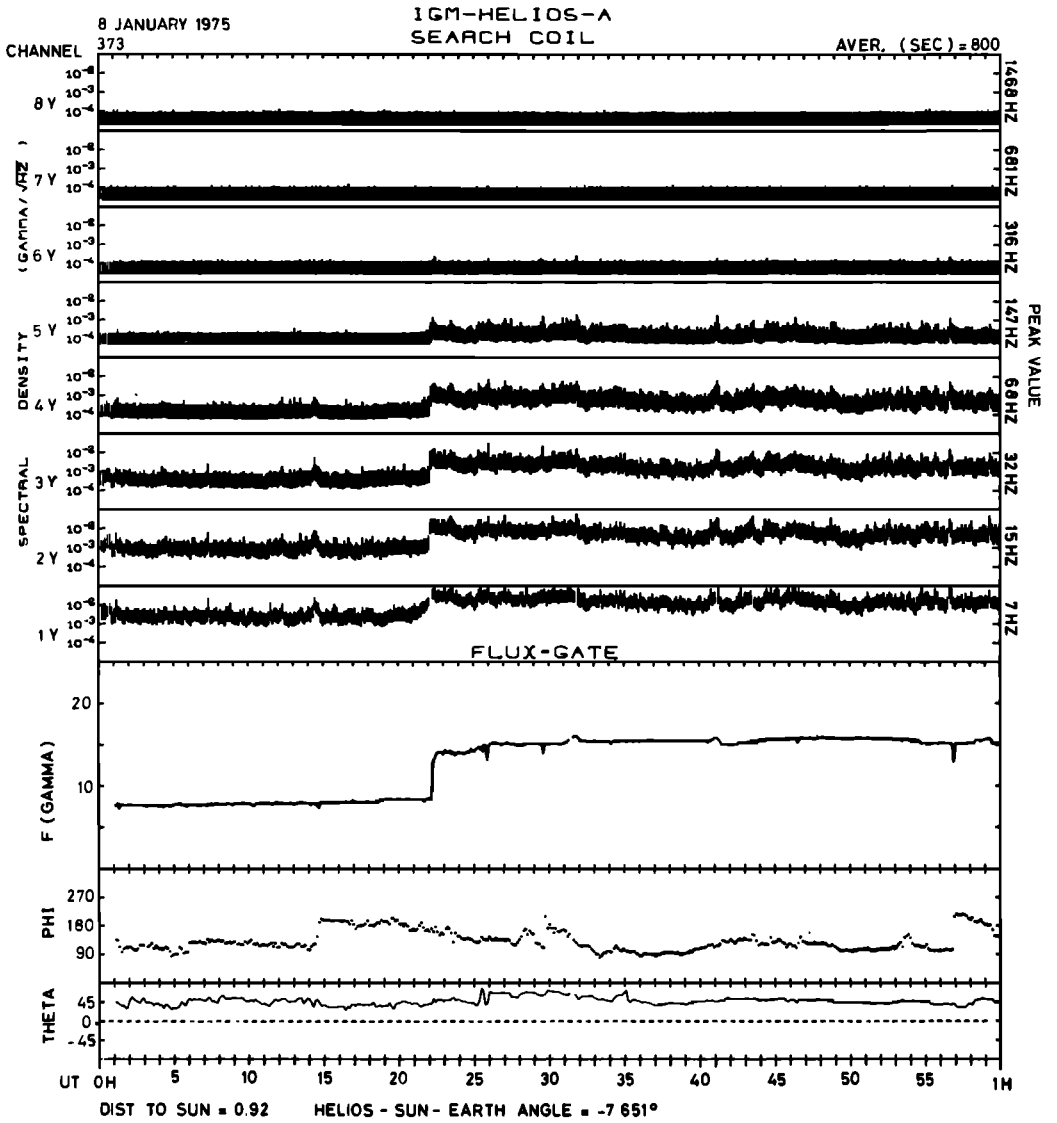

Fig. 9. Fast interplanetary shock of January 8, 1975, at 0022:09 in search coil and flux-gate data.

frame (e.g., 6.2.18 of *Jeffrey and Taniuti* [1964]) of $V_{n,1} = 114.8$ km/s. The Alfvén Mach number based on normal components is therefore $A_{n,1} = 1.57$. The normal speed behind the shock is $V_{n,2} = 64.8$ km/s, and the change in normal velocity $[V_n] = -50.0$ km/s. The change $[V_n]$ can also be obtained directly from the plasma observations. We obtain $[V_n] = -45.4$ km/s and $V_{n,1} = 104.3$ km/s or $A_{n,1} = 1.43$, which is in good agreement with the theoretical values. The shock propagation speed is then obtained to be $V_p = 520$ km/s in the direction of its normal **n**.

Time in Figures 9 and 10 can then be converted into a spatial variable x in the **n** direction in the shock frame by using $x = 520$ km/s $\times$ (0022:09 $- t$). It is more relevant to use a dimensionless scale. The length scale $c/\omega_{pi,1}$, where ω_{pi} is the plasma frequency of the protons, is 114 km ahead of the shock, and we may use $\xi = x\omega_{pi,1}/c$. Note that c/ω_{pi} is the gyroradius of a proton gyrating at the Alfvén speed.

Figure 10 contains high-time-resolution data of the shock with ξ as a second independent variable. It shows the fine structure of the shock in much more detail. Although the waves around $\xi = 150$ of 3-s period are not necessarily shock precursors, strong precursor wave activity occurs for $\xi < 50$, i.e., after 0022:00. It is not resolved in frequency by the flux gate and has peak to peak amplitudes of $\approx 1.5\ \gamma$ in magnitude. The precursors in the lowest wave channels are followed by steep increases with ratios $P_2(f_{cn})/P_1(f_{cn}) \approx 5$, ≈ 10, and 10 for channels 1Y, 2Y, and 3Y, respectively, and similar increases for channels 1Z, 2Z, and 3Z, which are not presented here. The dc fields after the shock transition show a remarkable laminar structure, particularly in magnitude, with superposed wave fields. The period of the laminar structure is ~4 s or $\Delta\xi \approx 18$ or 24 proton gyroradii behind the shock. It is also remarkable in this example that there is a jump in spectral densities and peak values for each 1.125-s interval but no maximum in these values for the shock transition, except possibly for channels 1Y and 1Z.

The peak value in channel 1Y corresponds to $\dot{Y} \approx 10^{-1} \times 7 \times (5.3)^{1/2} \times 2\pi = 10\ \gamma$/s in the frequency range from 4.7 to 10 Hz. At the same time the Z component yields $\approx 15\ \gamma$/s. If we think of this shock as consisting of a laminar propagating profile with superposed irregular wave fields, the shock 'thickness' cannot be less than about 0.25 s or $\Delta\xi \approx 1$, since we know the size of the jump to be equal to $\Delta\mathbf{B}$. Otherwise, stronger peak values should be expected. Since the ramp structure is not

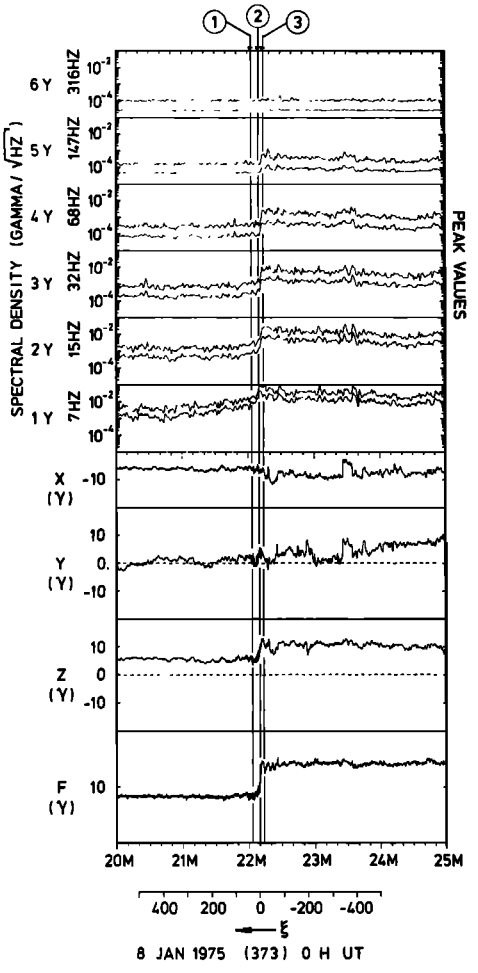

Fig. 10. High-time-resolution shock data with four vectors per second for flux-gate vector data and an averaging interval of 1.125 s for spectral data. ξ is the distance from the shock in units of a proton gyroradius c/ω_{pi} ahead of the shock. The shock was on January 8, 1975, at 0022:09. The times of the spectra shown in Figure 11 are indicated.

resolved by the flux gate with four vectors per second, the thickness must be very close to 0.25 s, i.e., 1 proton gyroradius. It is also consistent with this interpretation that the steep increases in average and peak values for channel 1Y coincide with the magnetic field transition observed by the flux gate, whereas it occurs somewhat later for channels 2Y–5Y.

Finally, Figure 11 shows three spectra of the Y component in the precursor region (curve 1), the shock transition (curve 2), and the shock wake region (curve 3). Also shown is the background noise level. In addition, the electron cyclotron frequencies $f_{ce,1}$ and $f_{ce,2}$ as well as the lower hybrid frequencies $f_{lh,1}$ and $f_{lh,2}$ are indicated. The change of the spectrum from the precursor region to the wake region is apparent. From about 15 to 70 Hz the slope of the transition region spectrum is about identical to the wake spectrum. It is clearly distinct from the precursor region spectrum, which starts very steeply but then decreases with much less slope. The spectrum in the wake region can be described by $P(f) = 1\ (\gamma^2/\mathrm{Hz})\, f^{-3.64}$ with $f \gtrsim 5$ Hz in hertz. From the point of view of plasma physics it would be more useful to know the spectra in the shock frame. However, a transformation into the shock frame is not possible, since the wave vector spectrum is not known.

Conclusions

We have presented observations of magnetic field variations in the solar wind from dc to 2.2 kHz. They have been obtained by the flux-gate magnetometer (0–4 Hz) and search coil magnetometer (4–2200 Hz) of the Technical University of Braunschweig on Helios 1.

We can distinguish a slowly varying component of the fluctuation spectrum having a time scale of about 10 min or longer. Fast variations in spectral density superimposed on the slowly varying component are called events. In this paper we have considered events which also show a clear signature in the dc field. The presentation of other extremely interesting events that do not show up clearly in the dc magnetic field is postponed to a later study. We next describe the four types of events which have been illustrated by one observed example each.

1. Directional discontinuities may reflect part of an incident whistler wave spectrum, thereby causing a jump in wave intensity, i.e., the discontinuity may act as a wave guide boundary. This is due to the fact that wave normal surfaces change across the discontinuity.

2. A purely directional discontinuity is caused by field-aligned currents which may cause instabilities possibly enhanced by the exact non-Maxwellian shape of the particle distribution functions. This behavior is also observed in a large number of cases as a peak in the wave spectra. In the special case discussed in this paper the maximum relative speed between electrons and protons amounted to 0.8 of the Alfvén speed. The observed magnetic fluctuations may be related to the waves treated theoretically by *Gary et al.* [1976*b*]. If a magnetic discontinuity also reveals magnitude changes, the currents are not field aligned any more, and the stability problem is more complex.

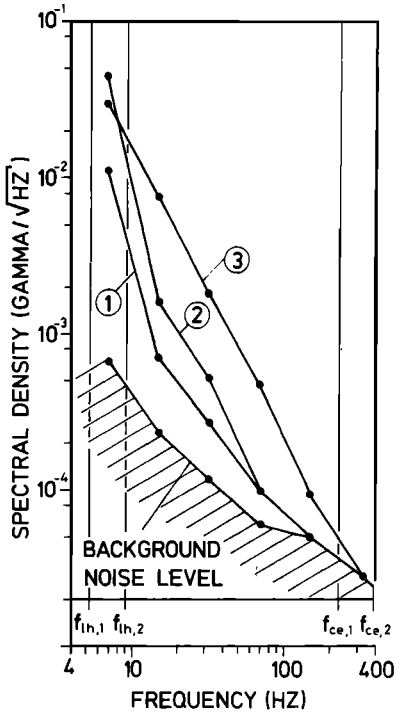

Fig. 11. Magnetic fluctuation spectra at times indicated in Figure 10. Curve 1 is a precursor spectrum, curve 2 a spectrum taken during the shock transition, and curve 3 a wake spectrum.

3. Reversible variations mostly connected with magnitude minima in the dc field occur on a time scale of 1 min. These 'dips' are often connected with appreciable maxima in wave intensity.

4. Interplanetary shocks are among the most dramatic events. Here we have discussed the fast shock which occurred on January 8, 1975, at 0022:09. This oblique shock had a ramp thickness of 1 proton gyroradius followed by some laminar structure. Precursor wave fields have been observed as well as wake fields. The shock jump is connected with a somewhat delayed jump in wave intensity, but there is essentially no peak in wave intensity above 10 Hz.

Whereas the analysis of shocks provides interesting observational material for the collisionless shock problem [*Galeev*, 1976], the first three types of events are interesting for the study of whistler wave propagation and generation by instabilities in the collisionless magnetoplasma of the solar wind. The numerous events of types 2 and 3 may contribute to the slowly varying background wave level when the distant contributions from several discontinuity wave sources sum up.

Acknowledgments. We are grateful to H. Rosenbauer, R. Schwenn, and H. Miggenrieder for making some of their plasma data available for this study before publication. In addition, we appreciate the hardware and software contributions of F. Gliem, A. Maier, J. Wawretzko, D. Lukoschus, E. Lammers, H. Barnstorf, H. Lange, and numerous other individuals to the experiments of the Technical University of Braunschweig. The work was supported by the Bundesministerium für Forschung und Technologie under the Helios program.

The Editor thanks W. C. Feldman and E. J. Smith for their assistance in evaluating this paper.

REFERENCES

Baader, H.-R., W. G. Pilipp, and H. J. Völk, Heat current and anisotropy-driven instabilities in connection with the solar wind, *J. Geophys. Res., 78,* 6737, 1973.

Barnes, A., Collisionless damping of hydromagnetic waves, *Phys. Fluids, 9,* 1483, 1966.

Behannon, K. W., Variation of the interplanetary magnetic field with heliocentric distance, *GSFC Rep. X-692-75-143,* Goddard Space Flight Center, Greenbelt, Md., 1975.

Beinroth, H. J., and F. M. Neubauer, Relationship between 'whistler wave' activity and the solar wind macrostructure (abstract), *Eos Trans. AGU, 57,* 672, 1976.

Beinroth, H. J., F. M. Neubauer, and G. Dehmel, Macroscale variations of whistler wave fields (abstract), *Eos Trans. AGU, 57,* 1000, 1976.

Burlaga, L. F., Micro-scale structures in the interplanetary medium, *Solar Phys., 4,* 67, 1968.

Burlaga, L. F., Hydromagnetic waves and discontinuities in the solar wind, *Space Sci. Rev., 12,* 600, 1971.

Burlaga, L. F., J. F. Lemaire, and J. M. Turner, Interplanetary boundary layers at 1 A.U., *GSFC Rep. X-692-76-168,* Goddard Space Flight Center, Greenbelt, Md., 1976.

Buti, B., Effects of solar wind composition, anisotropy, and streaming on ordinary mode electromagnetic instability, *J. Geophys. Res., 78,* 8023, 1973.

Cuperman, S., and R. W. Landau, Ion cyclotron resonant instability of rh waves propagating at an angle to the interplanetary magnetic field, *Astrophys. Space Sci., 5,* 333, 1969.

Dehmel, G., F. M. Neubauer, D. Lukoschus, J. Wawretzko, and E. Lammers, Das Induktionsspulen-Magnetometer-Experiment (E4), *Raumfahrtforschung, 19,* 241, 1975.

Fairfield, D. H., Whistler waves upstream from collisionless shocks, *J. Geophys. Res., 79,* 1368, 1974.

Fairfield, D. H., and W. C. Feldman, Standing waves at low Mach number laminar bow shocks, *J. Geophys. Res., 80,* 515, 1975.

Formisano, V., The earth's bow shock fine structure, in *Correlated Interplanetary and Magnetospheric Observations,* edited by D. E. Page, p. 187, D. Reidel, Hingham, Mass., 1974.

Formisano, V., and P. C. Hedgecock, Solar wind interaction with the earth's magnetic field, 3, On the earth's bow shock structure, *J. Geophys. Res., 78,* 3745, 1973*a*.

Formisano, V., and P. C. Hedgecock, On the structure of the turbulent bow shock, *J. Geophys. Res., 78,* 6522, 1973*b*.

Formisano, V., C. T. Russell, J. D. Means, E. W. Greenstadt, F. L. Scarf, and M. Neugebauer, Collisionless shock waves in space: A very high β structure, *J. Geophys. Res., 80,* 2013, 1975.

Forslund, D. W., Instabilities associated with heat conduction in the solar wind and their consequences, *J. Geophys. Res., 75,* 17, 1970.

Frandsen, A. M. A., R. E. Holzer, and E. J. Smith, Ogo search-coil magnetometer experiments, *IEEE Trans. Geosci. Electron., GE-7,* 61, 1969.

Fredricks, R. W., and F. L. Scarf, Effects of solar wind composition on the threshold for plasma instability in the transition region, *J. Geophys. Res., 70,* 4765, 1965.

Fredricks, R. W., C. F. Kennel, F. L. Scarf, G. M. Crook, and I. M. Green, Detection of electric-field turbulence in the earth's bow shock, *Phys. Rev. Lett., 21,* 1761, 1968.

Fredricks, R. W., F. V. Coroniti, C. F. Kennel, and F. L. Scarf, Fast time-resolved spectra of electrostatic turbulence in the earth's bow shock, *Phys. Rev. Lett., 24,* 994, 1970*a*.

Fredricks, R. W., G. M. Crook, C. F. Kennel, I. M. Green, and F. L. Scarf, Ogo 5 observations of electrostatic turbulence in bow shock magnetic structures, *J. Geophys. Res., 75,* 3751, 1970*b*.

Fredricks, R. W., F. L. Scarf, and L. A. Frank, Nonthermal electrons and high-frequency waves in the upstream solar wind, 2, Analysis and interpretation, *J. Geophys. Res., 76,* 6691, 1971.

Fredricks, R. W., F. L. Scarf, and I. M. Green, Distributions of electron plasma oscillations upstream from the earth's bow shock, *J. Geophys. Res., 77,* 1300, 1972.

Galeev, A. A., Collisionless shocks, in *Physics of Solar Planetary Environments,* edited by D. J. Williams, AGU, Washington, D. C., 1976.

Gary, S. P., W. C. Feldman, D. W. Forslund, and M. D. Montgomery, Electron heat flux instabilities in the solar wind, *Geophys. Res. Lett., 2,* 79, 1975*a*.

Gary, S. P., W. C. Feldman, D. W. Forslund, and M. D. Montgomery, Heat flux instabilities in the solar wind, *J. Geophys. Res., 80,* 4197, 1975*b*.

Gary, S. P., M. D. Montgomery, W. C. Feldman, and D. W. Forslund, Proton temperature anisotropy instabilities in the solar wind, *J. Geophys. Res., 81,* 1241, 1976*a*.

Gary, S. P., R. A. Gerwin, and D. W. Forslund, Electromagnetic current instabilities, *Phys. Fluids, 19,* 579, 1976*b*.

Gliem, F., G. Dehmel, G. Musmann, C. Türke, U. Krupstedt, and R. P. Kugel, Die Bordrechner der Helios-Magnetometer-Experimente E2 und E4, *Raumfahrtforschung, 20,* 16, 1976.

Greenstadt, E. W., C. T. Russell, F. L. Scarf, V. Formisano, and M. Neugebauer, Structure of the quasi-perpendicular laminar bow shock, *J. Geophys. Res., 80,* 502, 1975.

Hamasaki, S., Electromagnetic microinstabilities of plasmas in a uniform magnetic induction, *Phys. Fluids, 11,* 2724, 1968.

Helliwell, R. A., *Whistlers and Related Ionospheric Phenomena,* Stanford University Press, Stanford, Calif., 1965.

Hollweg, J. V., Waves and instabilities in the solar wind, *Rev. Geophys. Space Phys., 13,* 263, 1975.

Hollweg, J. V., and H. J. Völk, Two new plasma instabilities in the solar wind, *Nature, 225,* 441, 1970*a*.

Hollweg, J. V., and H. J. Völk, New plasma instabilities in the solar wind, *J. Geophys. Res., 75,* 5297, 1970*b*.

Holzer, R. E., M. G. MacLeod, and E. J. Smith, Preliminary results from the Ogo 1 search coil magnetometer: Boundary positions and magnetic noise spectra, *J. Geophys. Res., 71,* 1481, 1966.

Holzer, R. E., T. G. Northrup, J. V. Olson, and C. T. Russell, Study of waves in the earth's bow shock, *J. Geophys. Res., 77,* 2264, 1972.

Jeffrey, A., and T. Taniuti, *Non-Linear Wave Propagation,* Academic, New York, 1964.

Kennel, C. F., and F. L. Scarf, Thermal anisotropies and electromagnetic instabilities in the solar wind, *J. Geophys. Res., 73,* 6149, 1968.

Lemaire, J., and L. F. Burlaga, Diamagnetic boundary layers: A kinetic theory, *Astrophys. Space Sci., 45,* 303, 1976.

Montgomery, D. C., and D. A. Tidman, *Plasma Kinetic Theory*, McGraw-Hill, New York, 1964.

Montgomery, M. D., S. P. Gary, D. W. Forslund, and W. C. Feldman, Electromagnetic ion-beam instabilities in the solar wind, *Phys. Rev. Lett., 35,* 667, 1975.

Musmann, G., F. M. Neubauer, A. Maier, and E. Lammers, Das Förstersonden-Magnetfeldexperiment (E2), *Raumfahrtforschung, 19,* 232, 1975.

Neubauer, F. M., H. J. Beinroth, H. Barnstorf, and G. Dehmel, Initial results from the Helios 1 search coil magnetometer experiment, *Z. Geophys.*, in press, 1977.

Neugebauer, M., The enhancement of solar wind fluctuations at the proton thermal gyroradius, *J. Geophys. Res., 80,* 998, 1975.

Olson, J. V., R. E. Holzer, and E. J. Smith, High-frequency magnetic fluctuations associated with the earth's bow shock, *J. Geophys. Res., 74,* 4601, 1969.

Pilipp, W., and H. J. Völk, Analysis of electromagnetic instabilities parallel to the magnetic field, *J. Plasma Phys., 6,* 1, 1971.

Rehn, H. W., Transverse plasma waves in the solar wind close to the proton gyrofrequency, *Z. Geophys., 40,* 269, 1974.

Rodriguez, P., and D. A. Gurnett, Electrostatic and electromagnetic turbulence associated with the earth's bow shock, *J. Geophys. Res., 80,* 19, 1975.

Scarf, F. L., and R. W. Fredricks, Ion cyclotron whistlers in the solar wind, *J. Geophys. Res., 73,* 1747, 1968.

Scarf, F. L., and G. L. Siscoe, The Pioneer 9 electric field experiment, 2, Observations between 0.75 and 1.0 AU, *Cosmic Electrodynamics, 2,* 44, 1971.

Scarf, F. L., and J. H. Wolfe, Pioneer 9 plasma wave and solar plasma measurements for the August 1972 storm period, *J. Geophys. Res., 79,* 4179, 1974.

Scarf, F. L., J. H. Wolfe, and R. W. Silva, A plasma instability associated with thermal anisotropies in the solar wind, *J. Geophys. Res., 72,* 993, 1967.

Scarf, F. L., R. W. Fredricks, I. M. Green, and M. Neugebauer, Ogo 5 observations of quasi-trapped electromagnetic waves in the solar wind, *J. Geophys. Res., 75,* 3735, 1970*a*.

Scarf, F. L., R. W. Fredricks, and C. F. Kennel, AC electric and magnetic fields and collisionless shock structures, in *Particles and Fields in the Magnetosphere*, edited by B. M. McCormac, p. 102, D. Reidel, Hingham, Mass., 1970*b*.

Scarf, F. L., I. M. Green, and G. M. Crook, The Pioneer 9 electric field experiment, 1, Near-earth observations, *Cosmic Electrodynamics, 1,* 496, 1971*a*.

Scarf, F. L., R. W. Fredricks, L. A. Frank, and M. Neugebauer, Nonthermal electrons and high-frequency waves in the upstream solar wind, 1, Observations, *J. Geophys. Res., 76,* 5162, 1971*b*.

Scarf, F. L., R. W. Fredricks, I. M. Green, and G. M. Crook, Observations of interplanetary plasma waves, spacecraft noise, and sheath phenomena on Imp 7, *J. Geophys. Res., 79,* 73, 1974.

Schwenn, R., H. Rosenbauer, and H. Miggenrieder, Das Plasma-experiment auf Helios (E1), *Raumfahrtforschung, 19,* 226, 1975.

Siscoe, G. L., L. Davis, P. J. Coleman, Jr., E. J. Smith, and D. E. Jones, Power spectra and discontinuities of the interplanetary magnetic field: Mariner 4, *J. Geophys. Res., 73,* 61, 1968.

Siscoe, G. L., F. L. Scarf, I. M. Green, J. H. Binsack, and H. S. Bridge, Very-low-frequency electric fields in the interplanetary medium: Pioneer 8, *J. Geophys. Res., 76,* 828, 1971.

Smith, E. J., Identification of interplanetary tangential and rotational discontinuities, *J. Geophys. Res., 78,* 2054, 1973.

Solodyna, C. V., J. W. Sari, and J. W. Belcher, Plasma field characteristics of directional discontinuities in the interplanetary medium, *J. Geophys. Res., 82,* 10, 1977.

Sonnerup, B. U. Ö., Magnetopause structure during the magnetic storm of September 24, 1961, *J. Geophys. Res., 76,* 6717, 1971.

Turner, J. M., L. F. Burlaga, N. F. Ness, and J. F. Lemaire, Magnetic holes in the solar wind (abstract), *Eos Trans. AGU, 57,* 320, 1976.

Unti, T. W. J., M. Neugebauer, and B. E. Goldstein, Direct measurements of solar wind fluctuations between 0.0048 and 13.3 Hz, *Astrophys. J., 180,* 591, 1973*a*.

Unti, T., M. Neugebauer, and C.-S. Wu, Shock system of February 2, 1969, *J. Geophys. Res., 78,* 7237, 1973*b*.

Watanabe, S., Anomalous dispersion relation and instability in the solar wind plasma with thermal anisotropy, *Rep. Ionos. Space Res. Jap., 24,* 298, 1970.

(Received September 2, 1976;
accepted March 16, 1977.)